

REVIEW

Electron microscope images of human coronaviruses

Reality versus illusion

Ghallab MA¹, Barsoum CH², Polak S³, El Hassoun O³, Ghallab AM^{2,4}

HPB and Liver Transplant Department, Queen Elizabeth Hospital, Birmingham, UK.
m.ghallab@nhs.net

ABSTRACT

Since the outbreak of COVID-19 as a pandemic disease earlier in 2020, several publications reported the electron microscope images of SARS-CoV-2. This article reviews 73 articles from March 1956 till April 2021, focusing on the ultrastructure characteristics of the coronaviruses. We present the scientific debate and provide an opinion on the current controversy of electron microscopic images interpreted as SARS-CoV-2 particles in specimens from patients with COVID-19. Finally, we report our findings in a post-mortem lung specimen of a COVID-19 patient. With this we hope to facilitate accurate interpretation of TEM findings, and contribute to the building of a unified database in the face of COVID-19 (Tab. 2, Fig. 8, Ref. 81). Text in PDF www.elis.sk

KEY WORDS: electron microscope, TEM, coronaviruses, SARS-CoV-2, COVID-19.

Abbreviations: Human coronaviruses (hCoV), Student code number 229E (229E), Organ culture 43 (OC43), Netherlands 63 (NL63), Hong Kong University 1 (HKU1), Severe acute respiratory syndrome-coronavirus (SARS-CoV), Middle East respiratory syndrome-coronavirus (MERS-CoV), Severe acute respiratory syndrome-coronavirus-2 (SARS-CoV-2), Coronavirus disease-2019 (COVID-19), Transmission electron microscope (TEM), Hematoxylin and eosin (HE), Infectious bronchitis virus (IBV), Human ciliated airway epithelial cell (HAE), Vero E6 cell (African green monkey embryonic kidney cells), Bronchial alveolar lavage (BAL), The National Institute of Allergy and Infectious Diseases, USA (NIAID), The Centers for Disease Control and Prevention, USA (CDC), Double-membrane vesicle (DMV).

Introduction

Identification of viruses using electron microscopy is based on their variable and distinct morphologies (1). At the beginning of a viral outbreak, it is important to identify the virus type and assess its novelty. This determines which approaches are better for detecting the causative agent, what helps in controlling its transmission and

limiting the potential consequences of the epidemic (2). Electron microscopy is an essential tool for the proper identification and study of coronaviruses based on their ultrastructural characteristics (3). “Corona” is a Latin word meaning crown, coronaviruses got this designation due to the presence of crown like spike peplomers surrounding viral particles as seen in negative stain preparations for the electron microscope (4). Currently, there are seven documented strains of coronavirus which cause infection in humans (human coronaviruses or hCoV), four of which usually cause mild cold-like symptoms. The first prototypic strain, hCoV-229E (alpha genera) was grown on standard tissue culture in 1967 (5, 6). The second was isolated using tracheal organ culture and found to be distinct from hCoV-229E, so it was named OC43 (beta genera) (7, 8). Early this century, two more hCoVs also causing mild symptoms were identified. In 2004, hCoV-NL63 (alpha genera) was isolated from the aspirate of a case with bronchiolitis in the Netherlands (9), while hCoV-HKU1 (beta genera) was isolated in Hong Kong from a patient with pneumonia in 2005 (10). There are, however, three more serious strains of hCoVs that were discovered during the 21st century, which cause severe acute respiratory illness or even death. These are; severe acute respiratory syndrome-coronavirus (SARS-CoV (beta genera)) in 2002–2003 (11), Middle East respiratory syndrome-coronavirus (MERS-CoV (beta genera)) in 2012 (12) and severe acute respiratory syndrome-coronavirus-2 (SARS-CoV-2 (beta genera)) in 2019–2020 which is the cause of coronavirus disease-2019 (COVID-19) (2, 13–19).

This article reviews the ultrastructural characteristics of the different strains of human coronaviruses with focus on the SARS-CoV-2, provides an opinion of the current debate concerning the presence of virus or virus-like particles in various organs and presents HE and TEM findings in lung samples of a post mortem case of COVID-19 pneumonia.

¹HPB and Liver Transplant Department, Queen Elizabeth Hospital, Birmingham, UK, ²Department of Histology, British University in Egypt (BUE), Egypt, ³Institute of Histology and Embryology, Faculty of Medicine, Comenius University, Bratislava, Slovakia, and ⁴Department of Histology, Faculty of Medicine, Zagazig University, Egypt

Address for correspondence: O. El Hassoun, Institute of Histology and Embryology, Faculty of Medicine, Comenius University in Bratislava, Spitalska 24, SK-813 72 Bratislava, Slovakia.
Phone: +421290119 284

Materials and methods

Since the outbreak of the COVID-19 pandemic, several publications reported electron microscopic images of SARS-CoV-2. Through a Google and Pubmed search, we reviewed 73 articles dealing with the ultrastructure of coronaviruses from March 1956 till April 2021, including author correspondence. We present the building of current body of knowledge on coronaviruses from an electron microscopic point of view, including the recent controversy on the interpretation of presence of SARS-CoV-2 virus/virus like particles in various organs. Based on our knowledge of the difficulty in demonstrating viral particles in autopsy specimens, we decided to test our hypothesis on lung tissue from a post mortem case with antigen-confirmed COVID-19 pneumonia. Lung tissue was taken from the right and left lung, upper and lower lobes. All tissue was processed for standard HE histology and TEM.

Morphology of Coronaviruses

Nine articles from the second half of the last century studied two known hCoVs at that time, hCoV-229E and hCoV-OC43. Twelve articles described electron microscopic images of the other two coronaviruses which cause cold-like symptoms, hCoV-NL63 and hCoV-HGU1. Twenty of the reviewed articles investigated electron microscope images SARS-CoV and MERS between 2003 and 2019. Finally, during 2020, more than forty articles and

reports were published concerning electron microscopic images of SARS-CoV-2, at a rate of almost one publication per week.

hCoV-229E

During the second half of the 20th century, ultrastructure of the infectious bronchitis virus (IBV) strains in chicken was examined by transmission electron microscope (TEM) with negative staining technique. The particles were circular in shape with diameter between 80 and 120 nm. Most of these particles had spike-like projections on the surface, attached to the virus by a narrow neck and sometimes forming a bulbous mass. Based on this, it was suggested that the infectious bronchitis virus was similar to the influenza virus in size and shape (7, 20–22). The 229E virus was isolated from an acute specimen obtained during an upper respiratory infection and was named after a student specimen coded 229E at the University of Chicago. It was cultured on WI-38 human diploid fibroblasts and was examined by thin section TEM. The viral particles were spherical, 80 to 100 nm in diameter, and contained a “hollow” or electron-transparent central area 35 to 50 nm in diameter. Virions were seen inside dilated vesicles and cisternae of rough endoplasmic reticulum (Fig. 1A) (5). There were some similarities observed between the 229E and IBV initially in organ cultures inoculated with specimens from human respiratory illnesses. However, examination after positive staining in ultrathin sections revealed a difference in their internal structure (6). The characteristic club-like structures around the particles which were readily apparent by negative staining were at times also visible in thin sections (23). Recent electron microscopic studies showed that hCoV-229E was spherical in shape with a diameter of 80 to 120 nm and with the nucleocapsid diameter from 9–13 nm. Virions were demonstrated inside dilated vesicles and cisternae of rough endoplasmic reticulum (24).

hCoV-OC43 (B814)

The B814 strain was isolated from nasopharyngeal wash of a patient with the common cold and grown in tracheal organ cultures and consequently was named OC43. In electron microscopic images, viral particles showed an overall diameter of 160 nm and characteristic spikes 20 nm in length (Fig. 1B) (7, 8). HCoV-OC43 was morphologically indistinguishable from CoV-226E and IBV, and patients infected with the virus presented similar clinical symptoms as that of 229E, with no serological cross-reactivity between both strains (25–27). Another strain of coronavirus similar to OC43 was detected using immune electron microscopy in organ culture harvests derived from a bronchial washing from an adult with an acute upper respiratory tract disease (28).

hCoV-NL63

In 2003, a novel virus was isolated from a child suffering from respiratory disease in the Netherlands. The virus was isolated and grown on a monkey kidney cell line and identified as hCoV-NL63 (29). The virus particles were successfully visualized in hCoV-NL63 infected human ciliated airway epithelial (HAE) cell cultures using TEM (30). The viral particles were seen in the cell cytoplasm close to the apical supranuclear region and inside

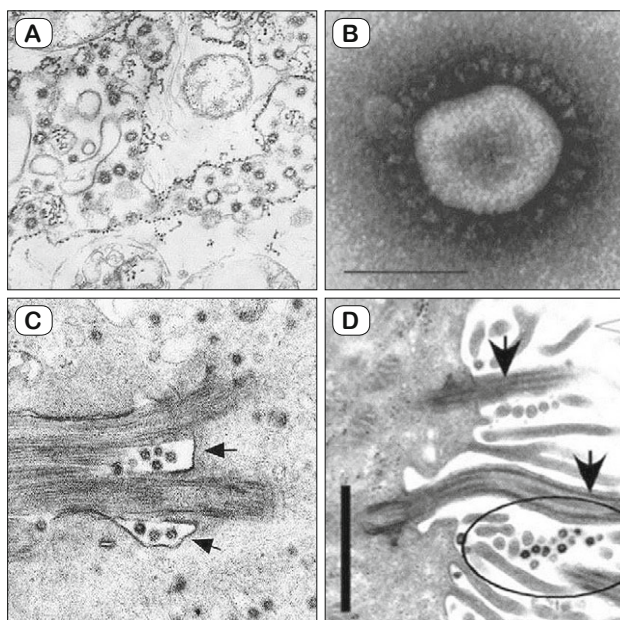


Fig. 1. (A) HCoV-229E particles within dilated vesicles of rough endoplasmic reticulum, 80 - 100 nm in diameter. X61,600 (5). © Permission License Number 4905830317744. (B) Negative stained hCoV-OC43 virus showing characteristic “club-shaped” surface projections. Bar=100 nm (8). (C) HCoV-NL63 particles surround the base of two cilia (arrows) of HAE culture $\times 146,000$ (30). © License Number 4944370304842. (D) HAE infected with HCoV-HKU1 showing the presence of the large numbers of virions (circled) associated with the surfaces of ciliated cells. Scale bar=2 μm (31). © Permission License Number 4936301017887.

Tab. 1. Virus particle morphology for each type of coronavirus with emphasis on SARS-CoV-2.

Virus	Reference	Visualised on	Time after inoculation	Diameter nm	Shape and surface	Centre	Location	Comment
hCoV-229E	5	fibroblast culture	6–72 hrs	80–100	Spherical, Club shaped spike projections	hollow 30–35nm	vesicles and ER cisternae	Morphologically identical to 229E
hCoV-OC43	7	tracheal organ culture	4 days	160	Club shaped spikes of 20 nm	spherical, core either clear, with electron dense granules, or totally electron dense	viewed in negative staining	cells in culture ranged from healthy to necrotic
hCoV-NL63	9	monkey kidney cells, human ciliated airway epithelial cells	5–6 days	75–115, mean 100	Spherical, long club-shaped, spikes 10–20 nm		Extracellularly around ciliae and in cytoplasm in apical supranuclear region and in rough ER	
hCoV-HKU1	31	human ciliated airway epithelial cells	72 hrs		Spherical with halo		extracellular associated with ciliae and in cytoplasm in small vesicles	
SARS-COV	35	Vero E6 cell, bronchial alveolar lavage (BAL)	3–5 days	78 mean	Spherical particles with club shaped viral projections, average 14 nm in length	electron-lucent	outer surface of plasma membrane, nucleocapsids in the rough endoplasmic reticulum/Golgi region and on the outer layer of nuclear envelope, nucleocapsids seen as black dots were seen in membrane-bound vesicles double-membrane vesicles and nucleocapsid inclusions	
MERS-CoV	40	Vero E6 culture			spherical particles with club-like projections emanating from the viral membrane		extracellularly near the plasma membrane, intracellularly inside cisternae of endoplasmic reticulum	
SARS-COV2	13	bronchoalveolar lavage inoculated on HAE, negative stained virus particles	6 days	60 to 140	spikes, about 9 to 12 nm	lucent with electron dense granules	Extracellular free virus particles and inclusion bodies filled with virus particles in membrane bound vesicles in cytoplasm	supported by PCR and sequencing
	44	nasopharyngeal oropharyngeal swab 3 post symptom onset inoculated on Vero cells.	2–3 days?		spherical	electron dense granules (nucleocapsid)	extracellular spherical particles	supported by PCR and sequencing
	45	Nasopharyngeal and oropharyngeal swab and sputum samples from symptomatic patients inoculated on Vero cells	48 hrs after inoculation	70–90	spherical	electron dense	wide range of intracellular organelles, especially in vesicles	supported by sequencing, particles determined by size.
	46	throat swab centrifuged	undetermined	70–80	Spherical with cobbled surface structure having envelope projections ending in round ‘peplomeric’ structures, averaged 15 ± 2 nm	electron dense	viewed in negative staining	patient tested with PCR

rough endoplasmic reticulum cisternae. In addition, hCoV-NL63 particles were seen surrounding the base of HAE cell cilia (Fig. 1C) (9, 30).

hCoV-HKU1

In 2005 the human coronavirus HKU1 was first discovered in an elderly patient, hospitalized with pneumonia and bronchiolitis, in Hong Kong (10). Human ciliated airway epithelial cell (HAE) cultures were used to grow hCoV-HKU1 successfully for the first time in vitro (31). To confirm the cellular localization of hCoV-HKU1, HAE cultures were inoculated with the isolated virus for 72 hours and then processed for TEM. Viral particles were observed in large amounts in association with the apical cilia and relatively fewer amounts were seen inside vesicles in the cytoplasm of HAE (Fig. 1D) (31). Most patients that were infected with hCoV-HKU1 presented with symptoms of respiratory tract infections (10, 26, 32, 33).

SARS-CoV

The WHO announced an outbreak of severe acute respiratory disease in China in November 2002. The novel virus causing this disease was termed severe acute respiratory syndrome coronavirus (SARS-CoV) (2, 34). Isolated viral samples from diseased patients in different countries were grown in Vero E6 cell (African green monkey embryonic kidney cells) cultures and examined by TEM

(3, 11). Large clustered viral particles measuring 80–140 nm in diameter with peripheral surface projections (20 nm) were identified adherent to the outer surface of the plasma membrane (3). Electron microscopic examination of cell cultures and of bronchial alveolar lavage (BAL) specimen identified viral nucleocapsids in the rough endoplasmic reticulum/Golgi region and on the outer layer of nuclear envelope. Spherical or occasionally pleomorphic virions acquired their envelope through budding into the cisternae of the endoplasmic reticulum. In infected Vero E6 cells SARS-CoV particles with nucleocapsids seen as black dots were seen in membrane-bound vesicles (Fig. 2A). SARS-CoV-infected cells showed double-membrane vesicles and nucleocapsid inclusions (Fig. 2B) (35, 36).

MERS-CoV

Another virulent human coronavirus emerged in the Middle East and was named Middle East respiratory syndrome coronavirus (MERS-CoV) (15, 37). This virus was first detected in 2012 from the lungs of a patient who died from severe respiratory disease. Since its discovery, clusters of secondary outbreaks have occurred due to the exportation of cases through travel (12, 33, 37, 38). The National Institute of Allergy and Infectious Diseases, USA (NIAID) and The Centers for Disease Control and Prevention (CDC) produced images of MERS coronavirus particles using TEM. Transmission electron micrographs of MERS-CoV particles found virions extracellularly near the plasma membrane of an infected Vero E6 culture cells and intracellularly inside cisternae of endoplasmic reticulum (Fig. 2C, D) (39, 40).

SARS-CoV-2

The WHO announced the outbreak of a novel coronavirus-2019 in Wuhan, China, with exportation to other countries in January 2020 (41). On March 11, 2020, the WHO declared coronavirus disease-2019 (COVID-19) a global pandemic, making severe acute respiratory syndrome coronavirus-2 (SARS-CoV-2) the first human coronavirus to cause a pandemic (42). A brief summary of this novel virus and disease was provided with references to the previously known SARS-CoV and MERS (2, 15, 16, 37, 43). In January 2020, Zhu and his colleagues published the first electron microscopic image of the virus isolated from the first patient in China (13). Electron microscopic images of the virus then were published from Korea (45), India (46), and the USA (44) The CDC published images of the virus isolated from the first USA COVID-19 patient in (47) (Fig. 3A). In February 2020, NIAID produced images of SARS-CoV-2 from the same patient using both scanning and transmission electron microscopes (48).

In all the above papers, SARS-CoV-2 infection was confirmed by PCR and/or sequencing methods. Specimens were collected from patients respiratory secretions and grown in cell cultures; HAE in (13) and various strains of Vero cells in (44, 45, 46) (Figs 3B, 4B). Virus particle morphology was demonstrated using negative TEM staining in (13, 46, 49) and is summarised in Table 1. Cell culture specimens were taken for electron microscopy at various intervals ranging from day 2 to 6 post infection. In HAE cultures, SARS-CoV2 particles were identified on the apical sur-

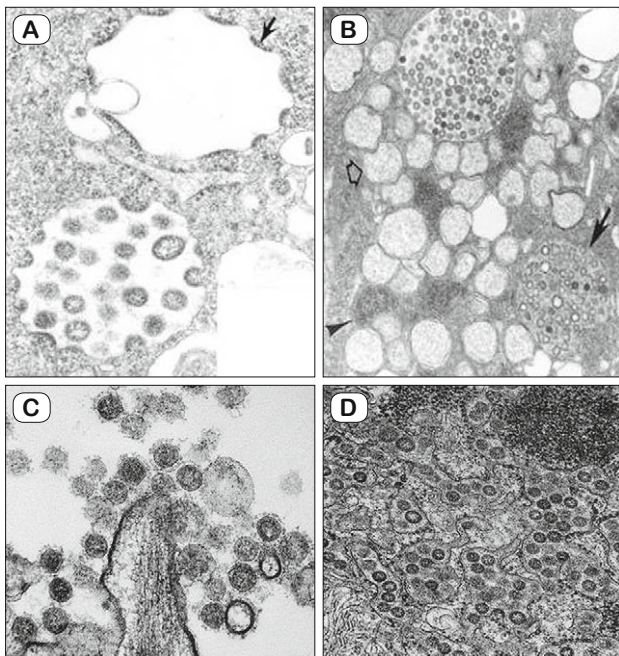


Fig. 2. (A) SARS-CoV particles with nucleocapsids appearing as black dots in infected Vero E6 cells seen budding into membrane-bound vesicles [35]. (B) SARS-CoV-infected cell with viral inclusion bodies (arrow) double-membrane vesicles (open arrow) and nucleocapsid inclusions (arrowhead). Bar = 100 nm. (35). © Permission from C. Goldsmith. Transmission electron micrographs of MERS-CoV particles in infected Vero E6 culture cells found (C) extracellularly and (D) intracellularly (39). © Free permission.

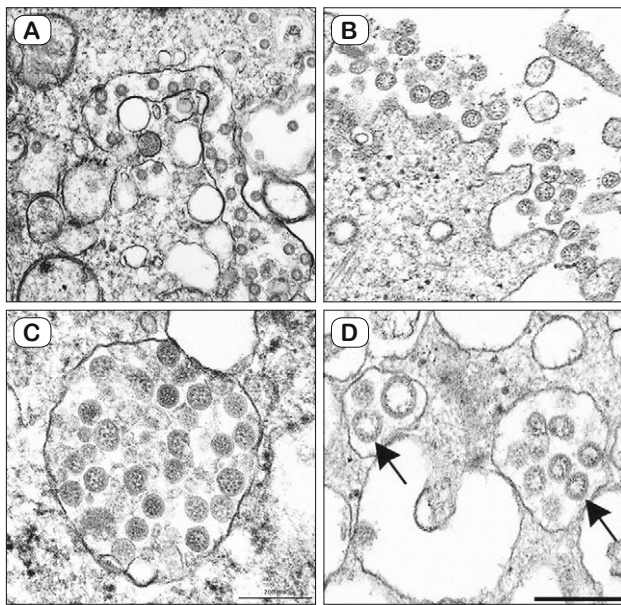


Fig. 3. (A) TEM image of SARS-CoV-2 isolated from the first U.S. case of COVID-19. The viral particles, contain cross-sections through nucleocapsids, seen as dark dots (47). © Free Permission. TEM images showing SARS-CoV-2 particles isolated and grown in a cell culture inoculated with infected patient nasopharyngeal and oropharyngeal fluids, showing extracellular spherical particles (B) with cross sections through the nucleocapsid, seen as black dots and intracellular particles (C,D) with a membrane coat around viral particles (44, 50, 51). © (B&C) Free Permission and (D) License Number 4916430084114.

face of both ciliated and secretory cells (Fig. 4A) and later inside both cell types, which as opposed to other types of coronaviruses is an evidence of its multicellular tropism (49).

SARS-CoV2 morphogenesis in cell cultures

Inclusion bodies were formed by viral components into pleomorphic double-membrane vesicles (DMVs). This description was identical to previous findings in both SARS-CoV and MERS-CoV (3, 13, 35, 48, 49). Spherical viral particles contained cross-sections through the nucleocapsids seen as black dots. Aggregates of virus particles were found in membrane-bound areas in the cisternae of the rough endoplasmic reticulum and Golgi complex, where the spikes would be located on the inside of the cisternae (Fig. 3C, D) (50, 51). TEM images demonstrated that SARS-CoV-2 entered cells through membrane fusion instead of endocytosis (24). Mature SARS-CoV-2 particles were released from the plasma membrane into the extracellular space when the smooth vesicles containing virions fused with the cell membrane (Fig. 4C, D) (24, 52). Several similarities in TEM images suggested that the life cycle of SARS-CoV-2 and SARS-CoV could be identical (11, 24, 52, 53).

Cytopathic effects of SARS CoV2

Changes in the ultrastructure of SARS-CoV2 HAE infected cells included the appearance of DMV, aggregates of denaturated mitochondria, enlarged apical ER, cilia shrinkage and immobility (49).

The induction of myelin like membrane whorls within the same vacuoles as the core particles in Vero E6 infected with SARS-CoV was described by (11). They also described the presence of electron dense donut shaped particles interpreted as the virus genome, either singly or in clusters of few particles enclosed in small vesicles in the cytoplasm or associated with the myelin-like figures. (24) described the presence of lamellar bodies in infected type II alveolar epithelial cells. (57) described vacuolisation of epithelial cells as a sign of viral infection.

SARS-CoV-2 particles by TEM, are they reality or illusion?

Many investigators claimed to have identified SARS-CoV-2 in biopsy or autopsy specimens from various organs of COVID-19 deceased patients. Post-mortem samples demonstrating virus like particles were taken from the lung, heart and kidney and examined with TEM (54-57). Purported virus particles were also shown in skin biopsies from COVID-19 patients (58), and were also demonstrated in lung, trachea, kidney and large intestine (62, 64). These findings however, have been challenged by scientists who argue that the particles seen in different organs are either misinterpreted or artefacts in electron microscopic images (50, 51, 59–63) (Fig. 5). Details of these papers and their responses are shown in Table 2.

Originally, the authors argued that the difference noticed in viral morphology by TEM can be attributed to a different virus activation/replication state or to the degeneration of the tissue and

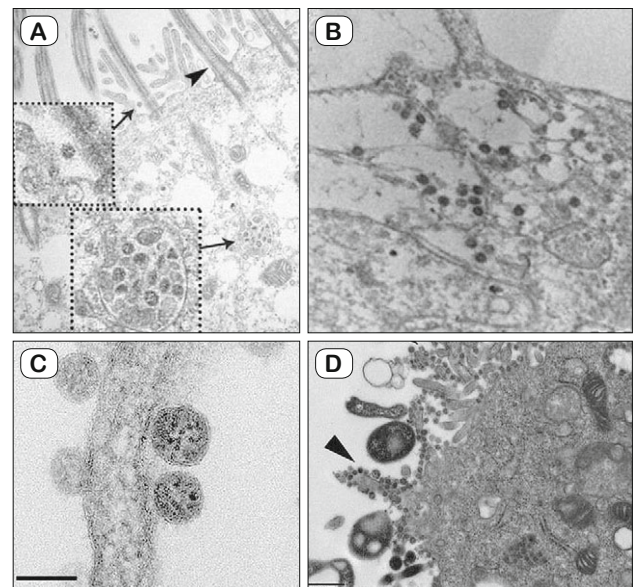


Fig. 4. (A) Infected HAE with SARSCoV-2 showing vesicles full of viral particles in ciliated cells and on the outer cell surface close to cilia (49). © Permission Free. (B) Thin section electron micrographs of Vero cells infected with SARS-CoV-2 showing aggregates of assembled intracellular virions (45). © Permission from corresponding author Myung-Guk Han. (C) Electron micrograph of Vero E6 cells infected with SARS-CoV-2 showing extracellular virus particles released outside the plasma membrane. Scale bars: 500 nm. (52). © Permission free. (D) Thin section electron micrographs of Vero E6 cells infected with a SARS-CoV-2-positive throat swab sample showing intracellular and extracellular viral particles. Bar=500 nm. (24). © Permission Free.

Tab. 2. Details of papers describing SARS-CoV-2 particles in various organs and challenging correspondence.

Author	Specimen type	Time taken	Sampled tissue	Methodology in sampled tissue	Findings	Conclusion	Response	Suggested interpretation
Pesaresi et al (54)	Post mortem	undetermined	heart kidney and lung	TEM	<ol style="list-style-type: none"> 1. Virions in extracellular vesicle, close to lung smooth muscle. 2. Intracellular virions in vesicles or associated to internal membrane (Fig 5b) 3. Virions in the cardiomyocytes adjacent to myofibrils 4. In renal epithelial tubular cell 	Virus enters cells of various organs	Bullock et al (72)	Multivesicular bodies, rough endoplasmic reticulum, undifferentiated structures
Varga et al (55)	Post mortem	Day 8 of symptoms	endothelial cells of various organs	Light microscopy and TEM	kidney tissue with viral inclusion bodies in a peritubular space and viral particles in endothelial cells of the glomerular capillary loops. (Fig. 5A)	SARS-CoV-2 induces endothelitis in several organs by direct viral involvement	Goldsmith et al (50)	Ribosomes on rough endoplasmic reticulum
Kissling et al (56)	biopsy	Day 8 of symptoms	kidney	Light microscopy, immunofluorescence, PCR, TEM	Vacuoles containing numerous spherical particles that may correspond to viral inclusion bodies in the podocyte cytoplasm (Fig 6D)	Direct viral toxicity in podocytes and tubular cells both of which harbor the ACE2 receptor	Miller et al (59), Bullock et al (72), Calomeni et al (61)	Multivesicular bodies
Farkash et al (57)	Post mortem	Day 6 of symptoms	PM kidney proximal tubules	Light microscopy, TEM	<ol style="list-style-type: none"> 1. Intracellular viruses arranged into arrays, suggestive of intracellular manufacture and assembly. 2. Presence of double membrane vesicles with possible viral assembly. 3. Vacuolation of epithelial cells after infection 	Direct viral involvement in acute renal injury of COVID-19 patients	Goldsmith et al (51), Bullock et al (72)	Clathrin coated vesicles, multivesicular bodies
Colmenero et al (58)	biopsy	Day 11 of symptoms	Acral skin lesions	Immunohistochemistry, TEM	<ol style="list-style-type: none"> 1. Virus-like particles in membrane-bound structures within the cytoplasm of endothelial cells. (Fig. 6C) 	pathogenetic role for SARS-CoV-2 in chilblains presenting during the pandemic	Brealey et al (63)	Clathrin coated vesicles
Bradley et al (62)	Post mortem	4 and 7 days	Lung, trachea, kidney, large intestine	Light microscopy, immunohistochemistry, TEM, RT-PCR	<ol style="list-style-type: none"> 1. Virions in tracheal epithelial cells, lung pneumocytes (Fig. 5D), enterocytes, and kidney endothelial cells and proximal tubular epithelial cells. Virions observed either outside cells, in close proximity to the cell membrane or inside the cells in aggregates confined within vesicles. Some particles were associated with double membranes resembling double membrane vesicles. 	<ol style="list-style-type: none"> 1. Diffuse alveolar damage is the major source of pulmonary injury 2. No evidence of widespread microvascular injury. 3. Possibility of extrapulmonary involvement in renal, intestinal, cardiac, and lymphoid tissues 	Dittmayer et al (68)	Multivesicular bodies
Su et al (64)	Post mortem	Not mentioned	kidney	Light microscopy, immunofluorescence, TEM	Virus-like particles in cytoplasm of renal proximal tubular epithelium (Fig. 5C), in podocytes, less so in distal tubules adjacent double membrane with surface projections, nucleocapsid apposing to the viral envelope, and the interior electron-lucent of the particles	Direct evidence of the invasion of SARS-CoV-2 into kidney tissue	Miller et al (59), Calomeni et al (61)	Clathrin coated vesicles, multivesicular bodies

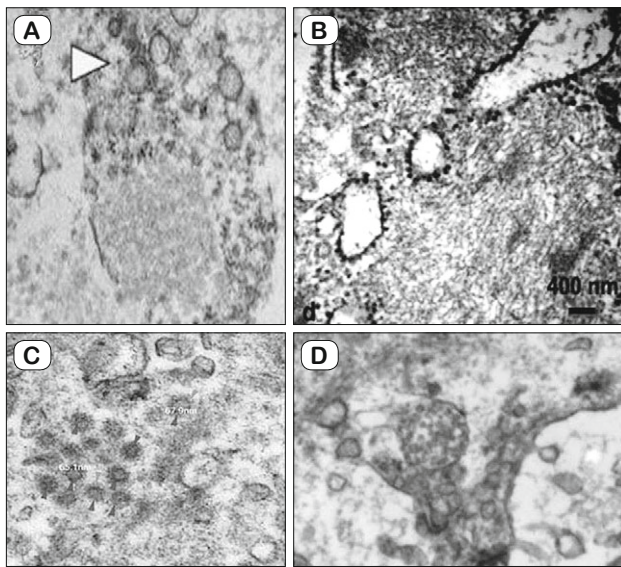


Fig. 5. (A) Electron microscopy of kidney endothelial cell from post-mortem autopsy of COVID-19 case, alleging to show viral inclusion bodies in peritubular space consistent with capillary containing purported viral particles. (55). © Permission License number 4918930272360. (B) TEM image from lung autopsy of COVID-19 positive case purporting to show viral particles associated to internal membranes. Bar=400 nm. (54). © Permission Free. (C) Ultrastructural features of kidneys from post-mortems of patients with COVID-19. Non-viral structures with distinctive spikes were present in the proximal tubular epithelium. (64). © Permission License Number 4916361209448. (D) Purported SARS-CoV-2 particles in kidney endothelial cells. Spherical structures were observed inside the cells in aggregates confined within double membrane vesicles (62). © Permission License Number 4924131458105.

cytolytic activity due to the release of lysosomal content (54). Several authors replied to the challenges, pointing out that challenging authors have studied coronavirus isolates grown in cell cultures (65), as opposed to routine EM processing of autopsy tissues under markedly different conditions (67). They underlined that they considered the identified structures to be possible, but not definitively proven, SARS-CoV-2 particles and changed the description in the preprint version article of “viral particle” to “coronavirus-like particle” (64, 65, 67). Authors argued that it remains unclear to what extent tissue type (cell culture, fresh biopsy material, or autopsy material), time to fixation, and post-mortal autolysis alter subcellular structures in preparation for EM (65), and emphasized that their findings point to a general host inflammatory response and could explain the vascular microcirculatory complications seen in different organs in patients with COVID-19 (65).

In agreement with the above mentioned dissenting opinions (50, 51, 59), more investigators (61, 68, 69) also disagreed with the interpretation and findings the above articles (54, 55, 58, 62, 64) and claimed that the electron microscopic images in those publications showed insufficient ultrastructural features of SARS-CoV-2. They concluded that not all apparent crowns are coronas and that some of these particles definitely represented clathrin-coated vesicles seen in podocytes, endothelial cells of the parietal glomerular epithelium, or multivesicular bodies (MVB), for which

they offered images (Fig. 6A, B) (61, 68, 69), this time using samples taken from autopsies (60, 68) and kidney biopsies (61, 69). Possible explanations of these misinterpretations include the varied size of MVB, ranging from 20 to 500 nm due to fusion of lysosomes with pinocytotic vesicles. In addition, Clathrin coated vesicles may give the false appearance of crown-like structures on electron microscopy. Therefore, images should show clear distinct ultrastructural features of SARS-CoV-2 particles and not just virus-like particles. It was concluded that examination of kidney biopsies by electron microscopy from patients with COVID-19-associated acute kidney injury, showed no evidence of direct SARS-CoV-2 infection (Fig. 7A, B, C, D) (60, 69).

Undisputed viral particles were demonstrated in the olfactory mucosa in individuals who died in the context of COVID-19 (70, 71). Bullock et al (72) published yet another extensive review of articles presenting structures misinterpreted for coronavirus particles. They also presented coronavirus images prepared from a deparaffinized sample after identification of the infected area using immunohistochemistry in autopsy tissue, with obvious compromise to viral particle morphology. They argued, that the presence of large numbers of intracellular and extracellular uniformly sized particles in areas corresponding to positive immunostaining or molecular labelling are clues to the presence of viruses. Members of the same team also published a guidance for identifying coronaviruses by TEM, including a description of mimicking organelles (73).

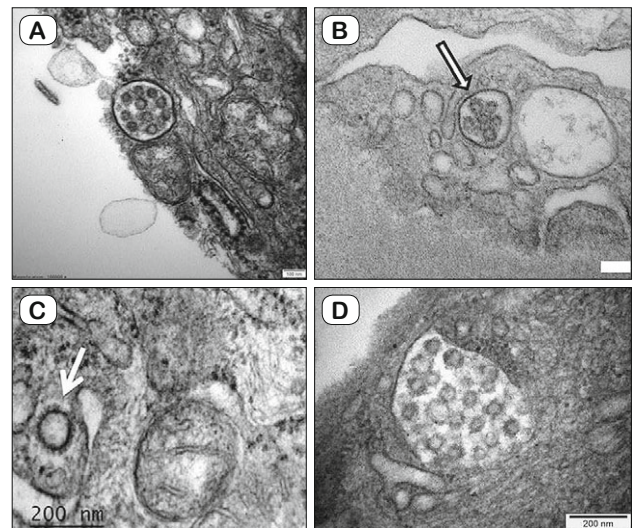


Fig. 6. (A) Multivesicular body in a podocyte of a patient with lupus nephritis who tested negative for COVID-19 (61). Bar=100 nm. © Permission License Number 4916960920151. (B) Renal biopsy from a patient with COVID-19 showing a podocyte containing a multivesicular body. (69). Bar=100 nm. © Permission License Number 4924190150506. (C) Ultrastructural image from skin biopsy of an endothelial cell showing alleged coronavirus-like particles (arrow). Bar=200 nm. (58). © Permission License Number 4924150616654. (D) Podocytes cytoplasmic vacuoles containing numerous spherical vesicles measuring between 50 to 110 nm and surrounded by spikes measuring 9 to 10 nm. These particles have been purported to correspond to viral inclusion bodies reported with the emerging SARS-CoV-2. Bar=200 nm. (56). © Permission License Number 4916420955619.

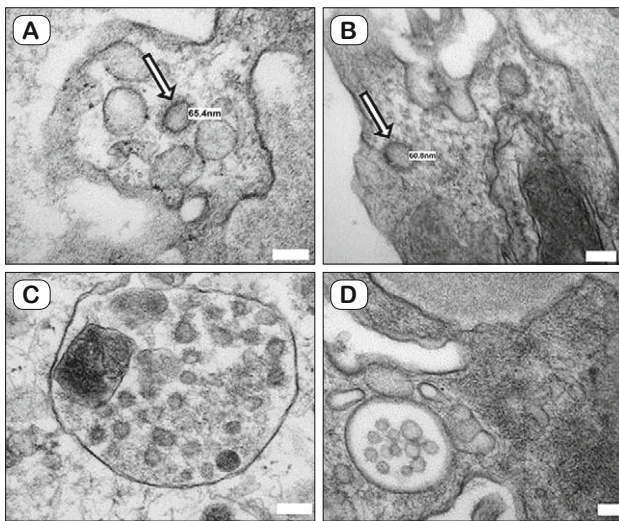


Fig. 7. (A) Renal biopsy from a patient positive for SARS-CoV2; showing endothelial cell containing a clathrin-coated vesicle with a “corona” 65 nm in diameter (white arrow); bar=100 nm. (B) Renal biopsy from a patient not infected with SARS-CoV2, showing an endothelial cell containing identical structures (white arrow); bar=100 nm. (C) Native renal biopsy from a patient with COVID-19 showing podocyte containing a microvesicular body/autophagosome (bar=100 nm). (D) Renal biopsy from a patient not infected with SARS-CoV2 showing microvesicular body in a podocyte (bar=100 nm). (69). © Permission License Number 4924190150506.

The recent review by Hopfer et al (74) aimed at combining multidisciplinary expertise of SARS-CoV-2 pathology, virology and electron microscopy. It emphasized that understanding virus biology is key for correct TEM interpretation. They offered TEM images of various stages of viral infection in culture cells and their morphological mimickers. The authors describe an area of convoluted membranes in an infected Vero cell as a sign of past viral replication, and present an image of an infected Vero cell with a replication organelle (74). Snijder et al (75) presented an extensive study of the replication of several types of coronaviruses in cell cultures, demonstrating convoluted membranes as a prominent element of beta coronavirus replication organelle.

Our case

An 83-year-old male with multiple comorbidities and one week history of flu symptoms with confirmed COVID-19 infection by antigen test was admitted to the hospital for severe unproductive cough, fever and progression of lower limb edema. Examination showed COVID-19 pneumonia with possible bacterial superinfection and cardiac decompensation in both circulations. The patient was treated with low flow oxygen, corticoids, antibiotics, diuretics and anticoagulants. Despite treatment, the patient continued to deteriorate and died on day 3 of hospitalization. Autopsy was performed the next day and samples were taken for standard HE histology and TEM. Specimens were processed for semithin sections and stained with toluidine blue to confirm presence of pneumocytes with cytopathic effect before proceeding with ultrathin sections.

Histology of the lungs showed acute interstitial pneumonia, proliferation of type II pneumocytes with marked cytopathic effect (Fig. 8A), alveolar spaces were filled with edema, hyaline membranes, epithelial cells and macrophages. A focal moderate lymphocytic infiltrate was seen in the interstitial space and some vessels contained microthrombi. In TEM, epithelial cells showed marked cytoplasmic vacuolisation (Fig. 8B), with abundant myelin like structures or lamellar bodies, in addition to dilation and disruption of rough endoplasmic reticulum (Fig. 8C). Few cells contained a system of membranes and vesicles in the perinuclear region which are suggestive of a replication complex. Fine browsing of the cytoplasm occasionally showed aggregates of convoluted membranes (Fig. 8D). Epithelial cells contained few undenaturated organelles, mostly in the perinuclear region. We did not demonstrate any viral particles in our material. Viable endothelial cells present in the specimen did not show signs of ultrastructural alteration or damage.

Our opinion

The article by Kissling et al (56) was criticized claiming that electron microscopy was the only alleged evidence presented in support of presence of virions in kidney tissue, while all other tests were negative (59). Carefully reading Kissling et al (56); the authors performed PCR for SARS-CoV-2 in sampled specimen and not only in the patient respiratory tract. Even though it came out negative, they point at the known limited rate of detection in nonrespiratory samples, and the poor quality of the extracted RNA material. They also performed immunofluorescence and excluded the presence of immune deposits to rule out other mechanisms.

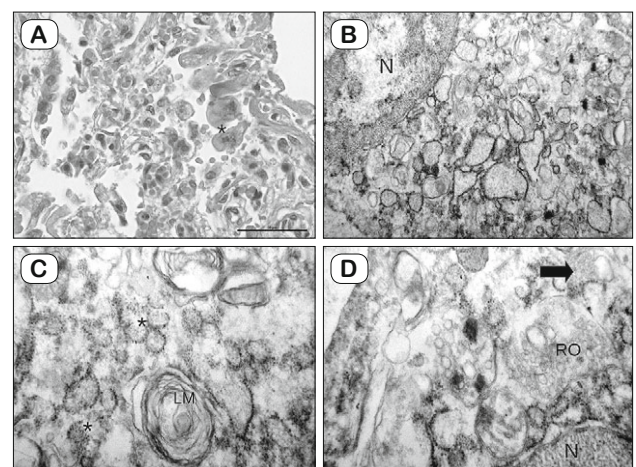


Fig. 8. Post mortem lung specimen from COVID-19 patient showing (A) proliferation of type II pneumocytes (asterisk) with marked cytopathic changes, HE. Bar=50 μ m. (B) Pneumocyte showing marked vacuolisation of the cytoplasm, N=nucleus. (C) formation of myelin like structures or lamellar bodies=LM, associated with double membrane vesicles in the cytoplasm. Asterisk shows dilated and disrupted rough endoplasmic reticulum. (D) system of membranes and vesicles in the perinuclear region suggestive of a replication organelle=RO in perinuclear region, N=nucleus. Arrow shows aggregates of convoluted membranes associated with past viral replication.

The authors explained that their hypothesis was based on the fact that observed morphologic changes in the kidney occurred with no obvious systemic injury. That is; acute tubular necrosis developed in the absence of hemodynamic compromise or severe pulmonary involvement, and collapsing focal segmental glomerulosclerosis (FSGS) occurred in a patient with normal levels of cytokines, in particular; interleukin-6. The authors went the extra mile and showed that the patient was homozygous for the at-risk apolipoprotein A (APO1) G1 variant (A342G and I348M), a recognized risk factor for the development collapsing FSGS in HIV and non-HIV patients. In our point of view, this report is an example of meticulous multidisciplinary approach with careful clinicopathological correlation and substantiated hypotheses.

Authors demonstrated immunohistochemical evidence of caspase in damaged tissue in COVID-19 patients as an indicator of apoptosis (55). Caspase is responsible for cleavage of several proteins involved in clathrin-mediated endocytosis, halting cargo uptake as part of the mechanisms of cell death (76). For this reason, we doubt the presence of an excessive amount of Clathrin coated vesicles in such an advanced stage of cell death as shown in figure 3a, b of (57). In our humble opinion, particles demonstrated in (64) are not in keeping with multivesicular bodies as interpreted in the (61) letter to the editor, as they are not bound by a limiting membrane.

Bradley et al (62) supported their findings by detecting SARS-CoV-2 RNA in lung, trachea, subcarinal lymph node, kidney, large intestine, spleen, liver, heart, and blood of patients sampled for TEM. They also demonstrated immunohistochemical positive staining of SARS-CoV-2 spike protein in renal tubular epithelium. Likewise, Colmenero et al (58) demonstrated positive granular staining of the spike protein in the cytoplasm of endothelial cells by immunohistochemistry. Although the spike protein is considered rather a safe antigen for immunohistochemistry, with described cross-reactivity only with other similar viral spike proteins (77), positive staining might not confirm the presence of entire viral particles. (78) demonstrated discordant negative spike protein staining by RNA ISH in cases with positive immunohistochemistry for the same protein. They suggested that cleaved spike protein may be deposited in endothelial cells and eccrine epithelium as a potential pathogenic mechanism of COVID-19 endotheliitis.

The lack of unequivocal evidence of virus particles in biopsy or postmortem specimens is not a proof that the virus was not there. A study of SARS-CoV2 shedding kinetics using cell cultures and PCR demonstrated a median shedding duration of 8 days post symptom onset, with drop below 5 % on day 12.5 (79). Taking this into consideration, in addition to factors compromising specimen quality, such as time to autopsy and tissue processing techniques, it is not surprising to find no evidence of viral particles. An extensive analysis comparing the presence of the virus with regard to time the specimen was taken after symptom onset, proof of infection and biopsy or post mortem is warranted. An attempt for such analysis will be limited due to poor and variable documentation of these facts within different reports.

Very few of the reviewed articles make reference to cytopathic ultrastructural changes in coronavirus infected cells (11, 24, 49,

57). In our material, these changes were immense, and corresponded to the cytopathic changes observed in HE. We believe that a demonstration of ultrastructural cytopathic changes post viral infection should be considered another tool for determining the population of affected cells, while bearing in mind structural alterations caused by apoptosis, necrosis and autolysis. The latter, could provide an explanation of the lack of significant abnormalities in endothelial cells in our specimen, where injured endothelial cells could have perished or disintegrated beyond recognition. Evidence of endothelial dysfunction with relation to COVID-19 infection in the literature is indisputable (80, 81), and the pathomechanisms involved are almost certainly multipronged. Meaning that the lack of evidence of viral particles within endothelial cells does not exclude viral induced injury.

Nowadays, virus detection by TEM is rarely used in routine setting, as it is expensive, time-consuming, covers minute portions of the tissue, and is not available in most laboratories (72).

However, TEM is still an essential tool and a front-line evaluation method in the search for unknown pathogens in outbreaks or epidemics (67). In studies of infectious diseases, TEM is still considered the gold standard to prove the presence of an infectious unit. It allows the exact localisation of viruses in tissues and within cells. This, in turn allows the determination of target cells of virus infection and informs about the reproduction of the virus (68). Virus visualisations using harvesting methods are excellent in purifying viruses from a sample and yielding a good amount for TEM. However, by using this method cellular and intracellular visualization and characterisation is lost. Finally, one of the limitations of working with cell cultures is the lack of host response analyses post viral infection. Nevertheless, such findings should improve the understanding of viral transmission and pathogenesis (49).

Conclusion

This article reviewed the available body of knowledge on the ultrastructure of coronaviruses and presented the scientific debate on the interpretation of TEM images of SARS-CoV-2 particles in biopsies or autopsies and their mimickers. Comparison between the two should facilitate accurate interpretation.

Demonstration of viral particles is not an easy task. It depends on a large number of variables, including time of inoculation, symptom onset, patient underlying conditions, genetic predisposition, choice of treatment and sampling parameters. In pandemic circumstances, scientists are under immense pressure to produce fast results in short time. Finding viral particles in various organs and tissues emerged as the holy grail of many researchers, with less attention paid to the biology of infected cells and virus replication mechanisms. We believe that a multifaceted approach should be adopted for the evaluation of any specimen, taking into consideration available clinicopathological correlations. Our suggestion for authors who were not able to demonstrate viral particles, but still have a good reason to believe in direct viral involvement, is to pursue ultrastructural changes in cells which are in keeping with post viral infection.

References

1. Curry A, Appleton H, Dowsett B. Application of transmission electron microscopy to the clinical study of viral and bacterial infections: present and future. *Micron* 2006; 37 (2): 91–106. DOI: 10.1016/j.micron.2005.10.001.
2. **Coronaviridae Study Group of the International Committee on Taxonomy of V.** The species Severe acute respiratory syndrome-related coronavirus: classifying 2019-nCoV and naming it SARS-CoV-2. *Nat Microbiol* 2020; 5 (4): 536–544. DOI: 10.1038/s41564-020-0695-z.
3. Ksiazek TG, Erdman D, Goldsmith CS, Zaki SR, Peret T, Emery S et al. A novel coronavirus associated with severe acute respiratory syndrome. *N Engl J Med* 2003; 348 (20): 1953–1966. DOI: 10.1056/NEJMoa030781.
4. Chorba T. The Concept of the Crown and Its Potential Role in the Downfall of Coronavirus. *Emerging Infectious Diseases* 2020; 26 (9): 2302–2230. DOI: 10.3201/eid2609.AC2609.
5. Hamre D, Kindig DA, Mann J. Growth and intracellular development of a new respiratory virus. *J Virol* 1967; 1 (4): 810–816. DOI: 10.1128/JVI.1.4.810-816.1967.
6. Becker WB, McIntosh K, Dees JH, Chanock RM. Morphogenesis of avian infectious bronchitis virus and a related human virus (strain 229E). *J Virol* 1967; 1 (5): 1019–1027. DOI: 10.1128/JVI.1.5.1019-1027.1967.
7. Almeida JD, Tyrrell DA. The morphology of three previously uncharacterized human respiratory viruses that grow in organ culture. *J Gen Virol* 1967; 1 (2): 175–178. DOI: 10.1099/0022-1317-1-2-175.
8. McIntosh K, Dees JH, Becker WB, Kapikian AZ, Chanock RM. Recovery in tracheal organ cultures of novel viruses from patients with respiratory disease. *Proc Natl Acad Sci USA* 1967; 57 (4): 933–940. DOI: 10.1073/pnas.57.4.933.
9. Orenstein JM, Banach B, Baker SC. Morphogenesis of Coronavirus HCoV-NL63 in Cell Culture: A Transmission Electron Microscopic Study. *Open Infect Dis J* 2008; 2: 52–58. DOI: 10.2174/1874279300802010052.
10. Woo PC, Lau SK, Chu CM, Chan KH, Tsoi HW, Huang Y et al. Characterization and complete genome sequence of a novel coronavirus, coronavirus HKU1, from patients with pneumonia. *J Virol* 2005; 79 (2): 884–895. DOI: 10.1128/JVI.79.2.884-895.2005.
11. Ng ML, Tan SH, See EE, Ooi EE, Ling AE. Early events of SARS coronavirus infection in vero cells. *J Med Virol* 2003; 71 (3): 323–331. DOI: 10.1002/jmv.10499.
12. Zaki AM, van Boheemen S, Bestebroer TM, Osterhaus AD, Fouchier RA. Isolation of a novel coronavirus from a man with pneumonia in Saudi Arabia. *N Engl J Med* 2012; 367 (19): 1814–1820. DOI: 10.1056/NEJMoa1211721.
13. Zhu N, Zhang D, Wang W, Li X, Yang B, Song J et al. A Novel Coronavirus from Patients with Pneumonia in China, 2019. *N Engl J Med* 2020; 382 (8): 727–733. DOI: 10.1056/NEJMoa2001017.
14. Cui J, Li F, Shi ZL. Origin and evolution of pathogenic coronaviruses. *Nat Rev Microbiol* 2019; 17 (3): 181–192. DOI: 10.1038/s41579-018-0118-9.
15. Ashour HM, Elkhatib WF, Rahman MM, Elshabrawy HA. Insights into the Recent 2019 Novel Coronavirus (SARS-CoV-2) in Light of Past Human Coronavirus Outbreaks. *Pathogens* 2020; 9 (3). DOI: 10.3390/pathogens9030186.
16. Hu B, Guo H, Zhou P, Shi ZL. Characteristics of SARS-CoV-2 and COVID-19. *Nat Rev Microbiol* 2020. DOI: 10.1038/s41579-020-00459-7.
17. Rodriguez-Morales AJ, Cardona-Ospina JA, Gutierrez-Ocampo E, Villamizar-Pena R, Holguin-Rivera Y, Escalera-Antezana JP et al. Clinical, laboratory and imaging features of COVID-19: A systematic review and meta-analysis. *Travel Med Infect Dis* 2020; 34: 101623. DOI: 10.1016/j.tmaid.2020.101623.
18. Gui M, Liu X, Guo D, Zhang Z, Yin CC, Chen Y et al. Electron microscopy studies of the coronavirus ribonucleoprotein complex. *Protein Cell* 2017; 8 (3): 219–224. DOI: 10.1007/s13238-016-0352-8.
19. **Microscope.com. Here's the Coronavirus Under an Electron Microscope:** [Microscope.com; 2020. https://www.microscope.com/coronavirus-under-an-electron-microscope/](https://www.microscope.com/coronavirus-under-an-electron-microscope/).
20. Morgan C, Howe C, Rose HM, Moore DH. Structure and Development of Viruses Observed in the Electron Microscope : Iv. Viruses of the Ri-Apc Group. *J Biophys Biochem Cytol* 1956; 2 (3): 351–360. DOI: 10.1083/jcb.2.3.351.
21. Berry DM, Cruickshank JG, Chu HP, Wells RJ. The Structure of Infectious Bronchitis Virus. *Virology* 1964; 23: 403–407. DOI: 10.1016/0042-6822(64)90263-6.
22. Tyrrell DA, Bynoe ML. Cultivation of a novel type of common-cold virus in organ cultures. *Br Med J* 1965; 1 (5448): 1467–1470. DOI: 10.1136/bmj.1.5448.1467.
23. Oshiro LS, Schieble JH, Lennette EH. Electron microscopic studies of coronavirus. *J Gen Virol* 1971; 12 (2): 161–168. DOI: 10.1099/0022-1317-12-2-161.
24. Zhao J, Zhou H, Huang W, Zhou J, Qiu M, Deng Z et al. Cell morphological analysis of SARS-CoV-2 infection by transmission electron microscopy. *J Thorac Dis* 2020; 12 (8): 4368–4373. DOI: 10.21037/jtd-20-1368.
25. Kin N, Miszczak F, Lin W, Gouilh MA, Vabret A, Consortium E. Genomic Analysis of 15 Human Coronaviruses OC43 (HCoV-OC43s) Circulating in France from 2001 to 2013 Reveals a High Intra-Specific Diversity with New Recombinant Genotypes. *Viruses* 2015; 7 (5): 2358–2377. DOI: 10.3390/v7052358.
26. Gaunt ER, Hardie A, Claas EC, Simmonds P, Templeton KE. Epidemiology and clinical presentations of the four human coronaviruses 229E, HKU1, NL63, and OC43 detected over 3 years using a novel multiplex real-time PCR method. *J Clin Microbiol* 2010; 48 (8): 2940–2947. DOI: 10.1128/JCM.00636-10.
27. Liu DX, Liang JQ, Fung TS. Human Coronavirus-229E, -OC43, -NL63, and -HKU1. Reference Module in Life Sciences2020.
28. Kapikian AZ, James HD, Kelly SJ, Vaughn AL. Detection of coronavirus strain 692 by immune electron microscopy. *Infect Immun* 1973; 7 (1): 111–116. DOI: 10.1128/iai.7.1.111-116.1973.
29. van der Hoek L, Pyrc K, Berkhout B. Human coronavirus NL63, a new respiratory virus. *FEMS Microbiol Rev* 2006; 30 (5): 760–773. DOI: 10.1111/j.1574-6976.2006.00032.x.
30. Banach BS, Orenstein JM, Fox LM, Randell SH, Rowley AH, Baker SC. Human airway epithelial cell culture to identify new respiratory viruses: coronavirus NL63 as a model. *J Virol Methods* 2009; 156 (1–2): 19–26. DOI: 10.1016/j.jviromet.2008.10.022.
31. Pyrc K, Sims AC, Dijkman R, Jebbink M, Long C, Deming D et al. Culturing the unculturable: human coronavirus HKU1 infects, replicates, and produces progeny virions in human ciliated airway epithelial cell cultures. *J Virol* 2010; 84 (21): 11255–11263. DOI: 10.1128/JVI.00947-10.

32. **Sloots TP, McErlean P, Speicher DJ, Arden KE, Nissen MD, Mackay IM.** Evidence of human coronavirus HKU1 and human bocavirus in Australian children. *J Clin Virol* 2006; 35 (1): 99–102. DOI: 10.1016/j.jcv.2005.09.008.
33. **Su S, Wong G, Shi W, Liu J, Lai ACK, Zhou J et al.** Epidemiology, Genetic Recombination, and Pathogenesis of Coronaviruses. *Trends Microbiol* 2016; 24 (6): 490–502. DOI: 10.1016/j.tim.2016.03.003.
34. **WHO.** Acute respiratory syndrome in China 2003 [https://www.who.int/csr/don/2003_2_20/en/].
35. **Goldsmith CS, Tatti KM, Ksiazek TG, Rollin PE, Comer JA, Lee WW et al.** Ultrastructural characterization of SARS coronavirus. *Emerg Infect Dis* 2004; 10 (2): 320–326. DOI: 10.3201/eid1002.030913.
36. **Goldsmith CS, Miller SE.** Modern uses of electron microscopy for detection of viruses. *Clin Microbiol Rev* 2009; 22 (4): 552–563. DOI: 10.1128/CMR.00027-09.
37. **Zhu Z, Lian X, Su X, Wu W, Marraro GA, Zeng Y.** From SARS and MERS to COVID-19: a brief summary and comparison of severe acute respiratory infections caused by three highly pathogenic human coronaviruses. *Respir Res* 2020; 21 (1): 224. DOI: 10.1186/s12931-020-01479-w.
38. **Assiri A, Al-Tawfiq JA, Al-Rabecah AA, Al-Rabiah FA, Al-Hajjar S, Al-Barrak A et al.** Epidemiological, demographic, and clinical characteristics of 47 cases of Middle East respiratory syndrome coronavirus disease from Saudi Arabia: a descriptive study. *The Lancet Infectious Diseases* 2013; 13 (9): 752–761. DOI: 10.1016/s1473-3099 (13)70204-4.
39. **NIAID.** MERS photos 2020 [updated January 23, 2020. https://www.nih.gov/news-events/news-releases/nih-officials-discuss-novel-coronavirus-recently-emerged-china.
40. https://www.rawpixel.com/image/2294226/free-photo-image-virus-cell-microscope.
41. **CDC.** Middle East Respiratory Syndrome (MERS) CDC: CDC; 2019 [cited 2019 October, 29]. https://www.cdc.gov/coronavirus/mers/photos.html.
42. **WHO.** Statement on the second meeting of the International Health Regulations (2005) Emergency Committee regarding the outbreak of novel coronavirus (2019-nCoV) 2020 [cited 2020 30 January]. https://www.who.int/news-room/detail/30-01-2020-statement-on-the-second-meeting-of-the-international-health-regulations-(2005)-emergency-committee-regarding-the-outbreak-of-novel-coronavirus-(2019-ncov).
43. **WHO.** Pandemic announcement, WHO Director-General's opening remarks at the media briefing on COVID-19 – 11 March 2020: WHO; 2020 [https://www.who.int/dg/speeches/detail/who-director-general-s-opening-remarks-at-the-media-briefing-on-covid-19---11-march-2020].
44. **WHO.** Coronavirus disease 2019 (COVID-19) Situation Report –94: WHO; 2020 [cited 2020 23 April]. https://www.who.int/docs/default-source/coronaviruse/situation-reports/20200423-sitrep-94-covid-19.pdf.
45. **Harcourt J, Tamin A, Lu X, Kamili S, Sakthivel SK, Murray J et al.** Isolation and characterization of SARS-CoV-2 from the first US COVID-19 patient. *bioRxiv* 2020. DOI: 10.1101/2020.03.02.972935.
46. **Kim JM, Chung YS, Jo HJ, Lee NJ, Kim MS, Woo SH et al.** Identification of Coronavirus Isolated from a Patient in Korea with COVID-19. *Osong Public Health Res Perspect* 2020; 11 (1): 3–7. DOI: 10.24171/j.phrp.2020.11.1.02.
47. **Prasad S, Potdar V, Cherian S, Abraham P, Basu A, Team I-NN.** Transmission electron microscopy imaging of SARS-CoV-2. *Indian J Med Res* 2020; 151 (2–3): 241–243. DOI: 10.4103/ijmr.IJMR_577_20.
48. **Bullock H A and Tamin A.** TEM SARS-CoV-2: CDC; 2020 [https://phil.cdc.gov/details.aspx?pid=23354].
49. **NIAID.** New Images of Novel Coronavirus SARS-CoV-2 Now Available – NIAID-RML National Institute of Allergy and Infectious Diseases – Rock Mountain Laboratories. Hamilton, Montana, USA.2020 [https://www.flickr.com/photos/niad/albums/72157712914621487].
50. **Zhu N, Wang W, Liu Z, Liang C, Wang W, Ye F et al.** Morphogenesis and cytopathic effect of SARS-CoV-2 infection in human airway epithelial cells. *Nat Commun* 2020; 11 (1): 3910. DOI: 10.1038/s41467-020-17796-z.
51. **Goldsmith CS, Miller SE, Martines RB, Bullock HA, Zaki SR.** Electron microscopy of SARS-CoV-2: a challenging task. *Lancet* 2020; 395 (10238): e99. DOI: 10.1016/S0140-6736 (20)31188-0.
52. **Miller SE, Goldsmith CS.** Caution in Identifying Coronaviruses by Electron Microscopy. *J Am Soc Nephrol* 2020; 31 (9): 2223–2224. DOI: 10.1681/asn.2020050755.
53. **Ogando NS, Dalebout TJ, Zevenhoven-Dobbe JC, Limpens R, van der Meer Y, Caly L et al.** SARS-coronavirus-2 replication in Vero E6 cells: replication kinetics, rapid adaptation and cytopathology. *J Gen Virol* 2020; 101 (9): 925–940. DOI: 10.1099/jgv.0.001453.
54. **Brahim Belhaouari D, Fontanini A, Baudoin JP, Haddad G, Le Bideau M, Bou Khalil JY et al.** The Strengths of Scanning Electron Microscopy in Deciphering SARS-CoV-2 Infectious Cycle. *Front Microbiol* 2020; 11: 2014. DOI: 10.3389/fmicb.2020.02014.
55. **Pesaresi M, Pirani F, Tagliabracci A, Valsecchi M, Procopio AD, Busardo FP et al.** SARS-CoV-2 identification in lungs, heart and kidney specimens by transmission and scanning electron microscopy. *Eur Rev Med Pharmacol Sci* 2020; 24 (9): 5186–5188. DOI: 10.26355/eur-rev_202005_21217.
56. **Varga Z, Flammer AJ, Steiger P, Haberecker M, Andermatt R, Zinkernagel AS et al.** Endothelial cell infection and endotheliitis in COVID-19. *Lancet* 2020; 395 (10234): 1417–1418. DOI: 10.1016/S0140-6736 (20)30937-5.
57. **Kissling S, Rotman S, Gerber C, Halfon M, Lamoth F, Comte D et al.** Collapsing glomerulopathy in a COVID-19 patient. *Kidney Int* 2020; 98 (1): 228–231. DOI: 10.1016/j.kint.2020.04.006.
58. **Farkash EA, Wilson AM, Jentzen JM.** Ultrastructural Evidence for Direct Renal Infection with SARS-CoV-2. *J Am Soc Nephrol* 2020; 31 (8): 1683–1687. DOI: 10.1681/ASN.2020040432.
59. **Colmenero I, Santonja C, Alonso-Riano M, Noguera-Morel L, Hernandez-Martin A, Andina D et al.** SARS-CoV-2 endothelial infection causes COVID-19 chilblains: histopathological, immunohistochemical and ultrastructural study of seven paediatric cases. *Br J Dermatol* 2020; 183 (4): 729–737. DOI: 10.1111/bjd.19327.
60. **Miller SE, Brealey JK.** Visualization of putative coronavirus in kidney. *Kidney Int* 2020; 98 (1): 231–232. DOI: 10.1016/j.kint.2020.05.004.
61. **Golmai P, Larsen CP, DeVita MV, Wahl SJ, Weins A, Rennke HG et al.** Histopathologic and Ultrastructural Findings in Postmortem Kidney Biopsy Material in 12 Patients with AKI and COVID-19. *J Am Soc Nephrol* 2020; 31 (9): 1944–1947. DOI: 10.1681/ASN.2020050683.
62. **Calomeni E, Satoskar A, Ayoub I, Brodsky S, Rovin BH, Nadasdy T.** Multivesicular bodies mimicking SARS-CoV-2 in patients without COVID-19. *Kidney Int* 2020; 98 (1): 233–234. DOI: 10.1016/j.kint.2020.05.003.

- 63. Bradley BT, Maioli H, Johnston R, Chaudhry I, Fink SL, Xu H et al.** Histopathology and ultrastructural findings of fatal COVID-19 infections in Washington State: a case series. *The Lancet* 2020; 396 (10247): 320–332. DOI: 10.1016/s0140-6736 (20)31305-2.
- 64. Brealey JK, Miller SE.** SARS-CoV-2 Has Not Been Detected Directly by Electron Microscopy in the Endothelium of Chilblain Lesions. *Br J Dermatol* 2020. DOI: 10.1111/bjd.19572.
- 65. Su H, Yang M, Wan C, Yi LX, Tang F, Zhu HY et al.** Renal histopathological analysis of 26 postmortem findings of patients with COVID-19 in China. *Kidney Int* 2020; 98 (1): 219–227. DOI: 10.1016/j.kint.2020.04.003.
- 66. Varga Z, Flammer AJ, Steiger P, Haberecker M, Andermatt R, Zinkernagel A et al.** Electron microscopy of SARS-CoV-2: a challenging task - Authors' reply. *Lancet* 2020; 395 (10238): e100. DOI: 10.1016/S0140-6736 (20)31185-5.
- 67. Su H, Gao D, Yang HC, Fogo AB, Nie X, Zhang C.** The authors reply. *Kidney Int* 2020; 98 (1): 232–233. DOI: 10.1016/j.kint.2020.05.007.
- 68. Kissling S, Rotman S, Fakhouri F.** The authors reply. *Kidney Int* 2020; 98 (1): 232. DOI: 10.1016/j.kint.2020.05.002.
- 69. Dittmayer C, Meinhardt J, Radbruch H, Radke J, Heppner BI, Heppner FL et al.** Why misinterpretation of electron micrographs in SARS-CoV-2-infected tissue goes viral. *The Lancet* 2020. DOI: 10.1016/S0140-6736 (20)32079-1.
- 70. Roufosse C, Curtis E, Moran L, Hollinshead M, Cook T, Hanley B et al.** Electron microscopic investigations in COVID-19: not all crowns are coronas. *Kidney Int* 2020; 98 (2): 505–506. DOI: 10.1016/j.kint.2020.05.012.
- 71. Meinhardt J, Radke J, Dittmayer C, Franz J, Thomas C, Mothes R et al.** Olfactory transmucosal SARS-CoV-2 invasion as a port of central nervous system entry in individuals with COVID-19. *Nat Neurosci* 2020. DOI: 10.1038/s41593-020-00758-5.
- 72. Lempriere S.** SARS-CoV-2 detected in olfactory neurons. *Nat Rev Neurol* 2021. DOI: 10.1038/s41582-020-00449-6.
- 73. Bullock HA, Goldsmith CS, Zaki SR, Martinez RB, Miller SE.** Difficulties in differentiating coronaviruses from subcellular structures in human tissues by electron microscopy. *Emerging Infect Dis* 2021; 27 (4): 1023.
- 74. Bullock HA, Goldsmith CS, Miller SE.** Best practices for correctly identifying coronavirus by transmission electron microscopy. *Kidney Int* 2021; 99 (4): 4–827.
- 75. Hopfer H et al.** Hunting coronavirus by transmission electron microscopy – a guide to SARS-CoV-2-associated ultrastructural pathology in COVID-19 tissues. *Histopathology* 2021; 78 (3): 358–370.
- 76. Snijder EJ et al.** A unifying structural and functional model of the coronavirus replication organelle: Tracking down RNA synthesis. *PLoS Biol* 2020; 18 (6): e3000715.
- 77. Austin CD et al.** Death-receptor activation halts clathrin-dependent endocytosis. *Proc Nat Acad Sci* 2006; 103 (27): 10283–10288.
- 78. Lean FZ et al.** Development of immunohistochemistry and in situ hybridisation for the detection of SARS-CoV and SARS-CoV-2 in formalin-fixed paraffin-embedded specimens. *Sci Reports* 2020; 10 (1): 1–9.
- 79. Ko CJ et al.** Discordant anti-SARS-CoV-2 spike protein and RNA staining in cutaneous pernioic lesions suggests endothelial deposition of cleaved spike protein. *J Cutaneous Pathology* 2021; 48 (1): 47–52.
- 80. van Kampen JJ et al.** Duration and key determinants of infectious virus shedding in hospitalized patients with coronavirus disease-2019 (COVID-19). *Nature Commun* 2021; 12 (1): 1–6.
- 81. Bonaventura A et al.** Endothelial dysfunction and immunothrombosis as key pathogenic mechanisms in COVID-19. *Nature Rev Immunol* 2021; 21 (5): 319–329.
- 82. Kaur S et al.** The enigma of endothelium in COVID-19. *Front Physiol* 2020; 11, 989.

Received January 20, 2021.

Accepted June 14, 2021.